



ELSEVIER

Earth and Planetary Science Letters 160 (1998) 845–862

EPSL

Post-breakup basaltic magmatism along the East Greenland Tertiary rifted margin

Stefan Bernstein^{a,*}, Peter B. Kelemen^b, Christian Tegner^{c,1}, Mark D. Kurz^d, Jurek Blusztajn^e,
C. Kent Brooks^f

^a Danish Lithosphere Centre, Øster Voldgade 10, DK-1350 Copenhagen K, Denmark

^b Woods Hole Oceanographic Institution, Woods Hole, MA, 02543, USA

^c Danish Lithosphere Centre, Øster Voldgade 10, DK-1350 Copenhagen K, Denmark

^d Woods Hole Oceanographic Institution, Woods Hole, MA 02543, USA

^e Woods Hole Oceanographic Institution, Woods Hole, MA 02543, USA

^f Geological Institute, University of Copenhagen, Øster Voldgade 10, DK-1350 Copenhagen K, Denmark

Received 6 February 1998; revised version received 3 June 1998; accepted 6 June 1998

Abstract

Mafic and ultramafic intrusions in East Greenland adjacent to the offshore Greenland–Iceland ridge were emplaced 5–9 My after continental breakup at 55 Ma [1]. Rare earth element (REE) concentrations determined by secondary ion mass spectrometry are reported for cumulus clinopyroxene from these intrusions, and the data are used to estimate REE abundance in equilibrium melts using available partitioning data. Estimated equilibrium melts from intrusions have strongly fractionated REE patterns with Nd/Dy(N) in the range 2 to 5.6 and Yb/Dy(N) 0.55 to 0.92, similar to values for coeval basalts. These melts have markedly higher Nd/Dy(N) than earlier breakup related flood basalts. The moderately low Yb/Dy(N) for the post-breakup volcanism is indicative of residual garnet in the source, while their high Nd/Dy(N) ratios can best be explained by aggregating low degree melts from a light-REE-enriched garnet- and spinel-bearing mantle source. We also report He, Sr, and Nd isotopic data for the intrusions. The highest ³He/⁴He ratios (>10 R/R_a) are found in the samples whose REE data reflect the largest proportion of melts from a garnet-bearing source, and having Sr and Nd isotopic compositions identical with the radiogenic Sr and unradiogenic Nd isotope end of the Iceland compositional field. There is no indication of a MORB-type mantle in the source of the intrusions. We postulate that post-breakup volcanism along the East Greenland coastline reflects the increasing proximity of the mantle plume to the East Greenland continental margin. The low degree of melting at high mean pressure inferred for the parental melts for the intrusions may reflect re-thickening of the lithosphere, which in turn was caused by the vigorous volcanism during breakup, with accompanying depletion of upper mantle and underplating of the crust at the continental margin. © 1998 Elsevier Science B.V. All rights reserved.

Keywords: basalts; igneous activity; continental drift; East Greenland; continental margin; Tertiary

* Corresponding author. Tel.: +45 3814 2656; Fax: +45 3311 0878; E-mail: sb@dlc.ku.dk

¹ Present address: Department of Earth Sciences, University of Aarhus, 8000 Århus C, Denmark.

1. Introduction

Formation of flood basalts is associated with continental rifting, commonly followed by formation of oceanic crust, and reflects voluminous magma production that may be linked to the presence of mantle diapirs or plumes (e.g. [2]). Following this tenet, early Tertiary magmatic activity in the North Atlantic borderlands has been related to the proto-Icelandic mantle plume at the time of rifting of the Eurasian continent [3]. In East Greenland, such magmatic activity is manifested as the Tertiary Scoresby Sund–Blosseville Coast plateau lavas. These are thick sequences of evolved tholeiites, erupted between 56 and 55 Ma during continental breakup [4–10]. A spreading center, which generated first seaward-dipping reflector sequences and later steady-state oceanic crust immediately off East Greenland, was established within magnetic anomaly C24r, around 56 Ma [11]. The erosional level in East Greenland, especially south of 68°N, exposes lithologies underlying the plateau basalts, such as extensive dyke swarms and large mafic and felsic intrusions (Fig. 1). Many of the mafic intrusions are gabbro complexes that experienced multiple replenishment episodes, and acted as low-pressure fractionation sites for basaltic melts [12–15]. Most were emplaced into the unconformity between the Precambrian basement and the flood basalts [16–18], commonly in the hinge zone of the coastal flexure [1,19]. New $^{40}\text{Ar}/^{39}\text{Ar}$ data [1,20] put these intrusions in a new and tectonically interesting context. Most are between 50 and 47 Ma, distinctly younger than continental breakup, and the formation of the main part of the Tertiary flood basalts in the region. Basalts coeval with the intrusions (the Igtertiva formation, ca. 49 Ma) crop out at Kap Dalton at 69°N [1,7,21]. Also, many basaltic dykes in the coast-parallel dyke swarm appear to postdate the breakup stage [22,23].

Basaltic magmatism at 50 to 47 Ma is difficult to understand in the context of continental rifting, because the Mid-Atlantic Ridge was a well-estab-

lished spreading center, ca. 150 km to the east, by this time (at anomaly 21; Fig. 1) [11]. Here we present new trace element data on clinopyroxenes, and He, Sr, and Nd isotopic data on mineral separates and whole-rock samples from the 50–47 Ma mafic intrusions that shed light on the reasons for post-breakup basaltic magmatism along the central East Greenland margin. Our data show that liquids forming the layered intrusions of East Greenland had high ratios of light to heavy REE, suggesting that their parental liquids formed by partial melting in the presence of garnet, indicating relatively high mean pressures of melting. This, and high $^3\text{He}/^4\text{He}$ ratios in some of the rocks, suggests that this magmatic activity was caused by the proximity of the Iceland mantle plume, maintaining melt generation at the continental margin after formation of oceanic crust in the North Atlantic was underway.

2. Experimental methods

Trace element analyses (Table 1) were made of clinopyroxene in thin sections of gabbroic and ultramafic rocks, using the Cameca IMS-3F ion microprobe at the Woods Hole Oceanographic Institution (WHOI) and methods described by Shimizu et al. [24]. Based on repeat analyses of clinopyroxene standards, we estimate that measured concentrations of REE are accurate to about $\pm 10\%$ relative. The clinopyroxenes from this study are all Ca-rich (20.41–23.86 wt% CaO). Mg# ($100 \times \text{Mg}/(\text{Mg} + \text{Fe})$ atomic) is in the range of 70–90 (Table 1; see also [12,14]).

Sr and Nd isotopic ratios were measured in clean mineral separates and a few additional bulk-rock samples (Table 2). Clinopyroxene mineral separates and whole rock chips were leached in hot 2.5 *N* HCl for 30 min, followed by 5 min in cold 5% HF and finally 30 min in hot 2.5 *N* HCl. Plagioclase mineral separates were leached in cold 2.5 *N* HCl for 10 min. Samples were then dissolved in a mixture

Fig. 1. Present day situation in the western North Atlantic. Shown in black are Tertiary intrusions. Those presented by name refer to mafic and ultramafic plutons that form the basis for this study. Also shown are the ODP Leg 152 and 163 Transects at about 63°N. Thin lines in the Denmark Strait are water depth contours in meters, while thick lines show magnetic anomalies at ca. 56 Ma (anomaly C24B, A) and at ca. 50 Ma (anomaly C21).

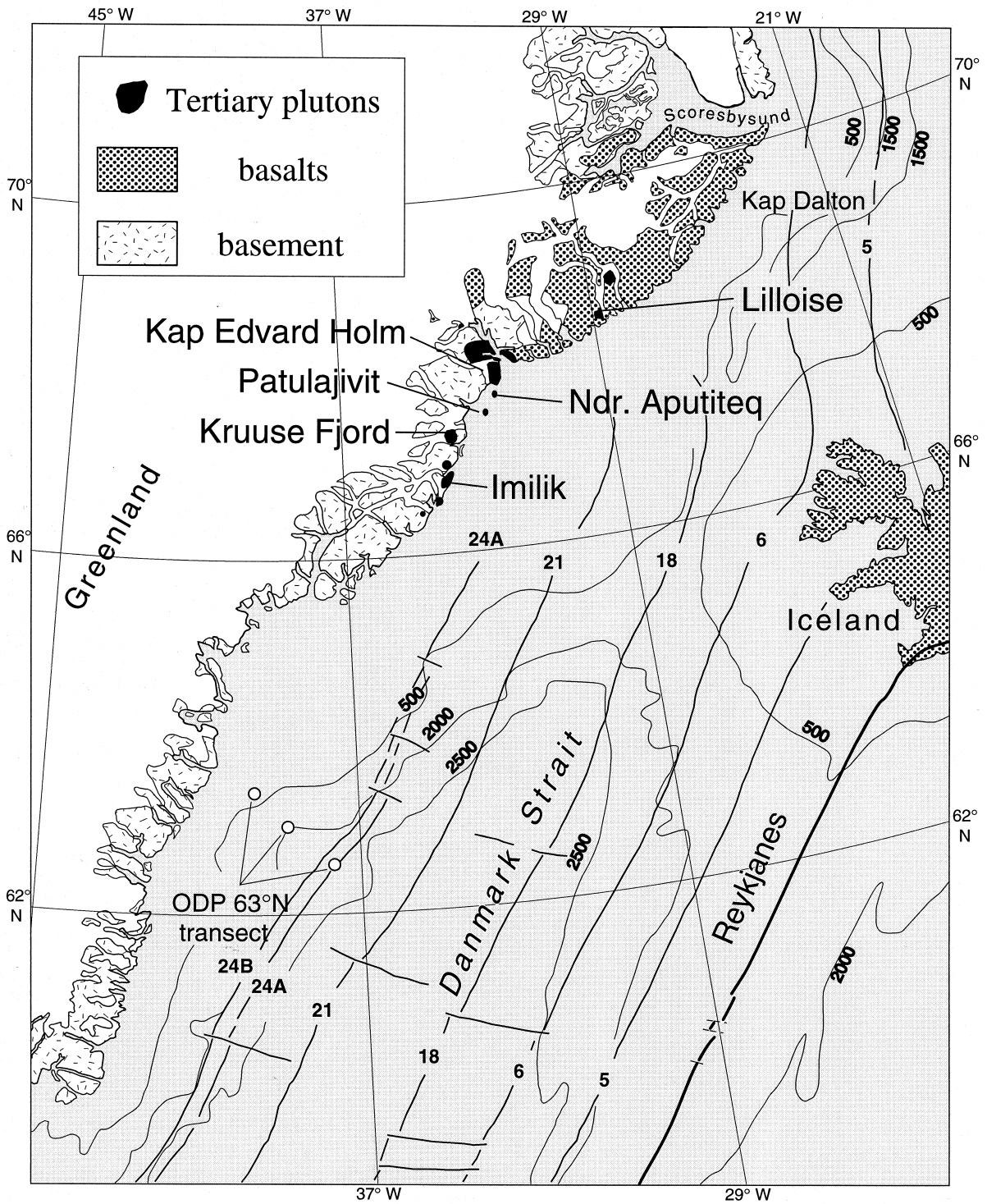


Table 1

Major and rare earth element concentrations in clinopyroxene from Tertiary mafic plutons along the East Greenland coast. The rare earth element data presented are average of two to four ion micro-probe analyses in crystal cores of cumulus clinopyroxenes

Lithology ^a : Sample No.:	Lilloise											KEH				
	u.b. KIMB2	gabbro 3366	u.b. KIMB12	gabbro 437336	perid. 437305	gabbro 533	gabbro 505gabb	wehrl. 504	wehrl. 437310	perid. 437329	wehrl. 73609	gabbro 73584	gabbro 3351	gabbro 312337	gabbro 312338	anort. 312383
SiO ₂ (wt%)	n.d.	51.82	49.94	49.61	53.40	n.d.	50.27	50.30	53.42	51.20	52.40	50.36	50.63	51.38	51.24	51.20
TiO ₂ (wt%)	n.d.	0.73	1.35	1.73	0.47	n.d.	1.09	1.07	0.37	1.66	0.61	1.28	1.37	1.18	1.33	0.94
Al ₂ O ₃ (wt%)	n.d.	2.12	4.13	4.40	1.30	n.d.	3.87	3.71	1.23	3.56	1.78	4.21	3.69	2.87	2.75	2.83
FeO (wt%)	n.d.	10.34	5.73	5.07	3.32	n.d.	5.49	5.76	3.43	6.78	3.49	6.13	7.39	8.32	7.98	7.83
MnO (wt%)	n.d.	0.36	0.10	0.19	0.01	n.d.	.14	0.12	0.01	0.21	0.08	0.14	0.17	0.09	0.15	0.20
MgO (wt%)	n.d.	13.70	14.24	14.53	16.78	n.d.	15.49	15.61	17.54	14.20	17.17	14.95	14.55	14.77	14.80	15.40
CaO (wt%)	n.d.	21.19	23.01	23.33	23.86	n.d.	22.98	22.50	23.25	22.01	23.63	23.58	21.82	20.97	21.33	21.30
Na ₂ O (wt%)	n.d.	0.38	0.43	0.43	0.50	n.d.	0.42	0.39	0.25	0.33	0.31	0.29	0.37	0.41	0.40	0.36
Cr ₂ O ₃ (wt%)	n.d.	0.00	0.32	0.39	0.56	n.d.	0.37	0.49	0.88	0.08	0.81	0.03	0.00	0.05	0.00	0.01
Sum		100.64	99.25	99.68	100.20		100.12	99.95	100.38	100.03	100.28	100.97	99.99	100.04	99.98	100.07
La (ppm)	1.52	8.84	3.48	3.98	1.54	3.87	2.66	3.20	0.37	5.63	1.71	3.01	3.15	2.03	1.11	1.56
Ce (ppm)	4.76	32.34	12.10	14.22	4.34	15.10	11.07	11.30	1.43	16.89	5.28	9.50	12.01	6.94	3.76	5.25
Nd (ppm)	3.85	27.37	10.70	12.60	3.48	14.55	11.84	10.96	1.59	11.56	4.33	8.02	11.55	6.48	3.31	5.20
Sm (ppm)	1.33	9.28	3.67	3.92	0.90	4.93	3.58	3.35	0.53	3.38	1.54	2.70	4.51	2.30	1.34	2.14
Eu (ppm)	0.45	2.25	1.26	1.42	0.43	1.67	1.42	1.30	0.24	1.13	0.54	1.05	1.31	0.87	0.48	0.78
Dy (ppm)	0.96	8.01	3.08	2.88	0.86	4.28	2.96	2.84	0.48	2.65	1.08	2.55	3.90	3.07	1.70	2.36
Er (ppm)	0.42	3.85	1.37	1.17	0.41	1.84	1.31	1.14	0.20	1.21	0.51	1.18	1.83	1.71	0.95	1.27
Yb (ppm)	0.38	3.22	1.11	1.10	0.35	1.68	1.21	1.10	0.21	1.09	0.41	0.94	1.43	1.63	1.02	1.38
Mg# in cpx	87.8	70.2	81.6	83.6	90.0	79.6	83.4	82.8	90.1	78.9	89.8	81.3	77.8	76.0	76.8	78.8
XAl _(T) in cpx		0.038	0.072	0.084	0.028		0.079	0.076	0.026	0.051	0.038	0.082	0.063	0.049	0.051	0.056
Mg# liq	62.3	35.2	50.5	54.0	67.4	47.3	53.6	52.6	67.7	46.2	66.8	50.0	44.7	42.1	43.2	46.1
Nd/Dy(N) liq	5.13	4.35	44.2	5.58	5.15	4.33	5.09	4.91	4.22	5.55	5.11	4.01	3.77	2.69	2.48	2.81
Yb/Dy(N) liq	0.60	0.62	0.55	0.58	0.62	0.60	0.62	0.59	0.67	0.63	0.58	0.56	0.56	0.81	0.92	0.89

Table 1 (continued)

Lithology ^a : Sample No.:	KEH wehrlite									Nordre Aputiteq			Patulajivit		Kruise Fjord	
	gabbro 312380	gabbro 352164	perid. 312361a 5	perid. 312361a 6	wehrl. 1610 2	wehrl. 1610 3	wehrl. 1610 c 4	wehrl. 1610 c 8	wehrl. 92365	gabbro AP 106A	gabbro AP 115	gabbro AP 116	gabbro P78A	gabbro P97	perid. KF 55	gabbro 71003
SiO ₂ (wt%)	50.71	51.88	51.08	51.93	51.73	52.26	51.56	51.83	51.64	50.09	51.03	51.29	51.66	51.13	51.22	51.48
TiO ₂ (wt%)	1.08	0.64	0.59	0.45	0.58	0.58	0.39	0.65	0.67	1.12	0.65	0.85	0.98	1.70	0.40	0.70
Al ₂ O ₃ (wt%)	3.18	2.22	3.60	3.87	3.51	3.44	3.68	3.20	3.48	4.16	3.31	3.24	2.66	3.31	4.65	2.77
FeO (wt%)	7.73	6.72	3.54	3.55	4.14	4.12	3.91	3.91	4.06	5.81	6.23	6.18	8.53	8.98	3.90	6.17
MnO (wt%)	0.11	0.03	0.00	0.01	0.07	0.12	0.20	0.01	0.09	0.00	0.23	0.06	0.09	0.21	0.03	0.01
MgO (wt%)	15.20	16.93	17.10	17.05	16.59	16.87	16.58	16.60	16.47	16.03	15.83	16.12	14.82	14.18	15.75	16.04
CaO (wt%)	21.20	21.28	22.54	22.38	22.47	22.27	22.53	22.31	22.12	21.99	22.07	21.86	20.58	20.55	22.76	22.03
Na ₂ O (wt%)	0.32	0.35	0.39	0.35	0.31	0.28	0.17	0.28	0.27	0.24	0.30	0.26	0.46	0.39	0.39	0.31
Cr ₂ O ₃ (wt%)	0.10	0.63	1.17	1.02	1.25	1.29	1.28	1.35	1.04	0.58	0.09	0.28	0.01	0.01	1.27	0.23
Sum	99.63	100.68	100.01	100.61	100.65	101.23	100.30	100.14	99.84	100.02	99.74	100.14	99.79	100.46	100.36	99.74
La (ppm)	1.22	1.47	0.40	0.61	0.99	1.07	1.97	2.64	2.12	1.14	1.73	1.61	2.27	1.40	1.06	0.72
Ce (ppm)	4.08	4.36	1.48	2.11	3.52	4.01	5.98	9.46	8.18	3.34	5.59	5.18	7.95	5.01	3.50	2.43
Nd (ppm)	4.09	4.45	1.53	2.47	3.24	4.07	5.39	8.98	8.43	3.04	5.02	5.18	8.96	5.15	3.21	2.54
Sm (ppm)	1.73	2.10	0.67	1.16	1.18	1.53	1.70	3.03	2.97	1.10	1.76	1.86	2.51	1.84	1.17	0.88
Eu (ppm)	0.57	0.71	0.31	0.35	0.42	0.45	0.62	1.02	1.05	0.28	0.55	0.54	1.10	0.66	0.42	0.37
Dy (ppm)	1.91	2.01	0.86	1.19	1.11	1.33	1.63	3.04	2.90	1.16	1.72	1.89	3.11	1.62	1.32	1.23
Er (ppm)	1.07	1.23	0.50	0.65	0.52	0.50	0.83	1.48	1.32	0.47	0.73	0.78	1.46	0.69	0.62	0.67
Yb (ppm)	0.94	1.20	0.51	0.70	0.43	0.54	0.58	1.24	1.12	0.64	0.84	0.94	1.29	0.64	0.57	0.61
Mg# in cpx	77.8	81.8	89.6	89.5	87.7	87.9	88.3	88.3	87.8	83.1	81.9	82.3	75.6	73.8	87.8	82.2
XAl _(T) in cpx	0.061	0.048	0.072	0.063	0.061	0.057	0.061	0.054	0.055	0.061	0.082	0.060	0.041	0.052	0.068	0.053
Mg# liq	44.6	50.8	66.4	66.3	62.2	62.7	63.5	63.5	62.4	53.1	51.0	51.7	41.6	39.3	62.3	51.6
Nd/Dy(N) liq	2.37	2.82	2.28	2.64	3.72	3.91	4.21	3.76	3.70	3.32	3.72	3.50	3.67	4.05	3.10	2.63
Yb/Dy(N) liq	0.75	0.91	0.91	0.89	0.60	0.62	0.54	0.62	0.59	0.84	0.75	0.76	0.64	0.61	0.66	0.75

Table 1 (continued)

Lithology ^a : Sample No.:	Kruuse Fjord		Imilik					Igtertiva Formation							
	troc.	troc.	gabbro	gabbro	gabbro	gabbro	gabbro	perid.	perid.	perid.	perid.	perid.	basalt	basalt	basalt
	71068	22227	416787	416718	416812	416851	416825	416799	416705	416829	416830	416804	116343	116344	116382
SiO ₂ (wt%)	51.24	51.35	52.64	51.29	51.23	50.97	51.67	51.58	52.91	50.92	52.28	52.40	49.83	49.14	48.95
TiO ₂ (wt%)	0.76	0.70	0.39	0.57	0.75	0.86	0.43	0.47	0.30	0.39	0.53	0.73	3.01	2.49	2.06
Al ₂ O ₃ (wt%)	3.91	3.19	2.81	2.56	2.71	2.79	3.07	4.02	2.65	4.24	3.32	1.91	13.35	14.19	13.96
FeO (wt%)	3.79	6.67	5.51	7.74	6.72	7.12	4.98	3.65	3.39	3.85	4.10	7.23	13.88	12.24	12.25
MnO (wt%)	0.01	0.05	0.24	0.20	0.18	0.24	0.23	0.01	0.01	0.01	0.01	0.27	0.24	0.22	0.20
MgO (wt%)	15.93	15.17	16.83	15.93	16.21	15.62	16.83	16.80	17.82	17.00	17.46	15.73	4.70	5.71	6.14
CaO (wt%)	22.44	21.87	21.67	20.41	21.56	21.33	21.80	22.01	22.63	21.69	21.52	22.05	9.66	10.83	11.56
Na ₂ O (wt%)	1.07	0.39	0.26	0.41	0.32	0.25	0.27	0.20	0.20	0.23	0.23	0.31	2.72	2.62	2.49
Cr ₂ O ₃ (wt%)	0.54	0.21	0.24	0.21	0.08	0.26	0.43	1.26	0.82	1.32	0.37	0.01			
Sum	99.69	99.60	100.59	99.32	99.76	99.44	99.71	100.00	100.73	99.65	99.82	100.64	97.39	97.44	97.61
La (ppm)	0.82	1.17	0.25	1.01	1.05	0.86	0.66	0.53	0.35	0.39	0.53	0.83	26.1	17.7	14.6
Ce (ppm)	2.90	4.31	0.91	3.93	3.64	3.33	2.55	1.97	1.19	1.57	2.10	3.54	55.3	38.9	31.1
Nd (ppm)	3.34	4.21	1.21	4.82	3.77	3.82	3.46	2.09	1.46	1.74	2.62	4.26	33.5	24.3	19.7
Sm (ppm)	0.84	0.67	0.61	1.19	1.26	1.06	1.29	0.75	0.73	0.69	0.74	0.99	8.2	6.6	5.1
Eu (ppm)	0.44	0.42	0.27	0.66	0.50	0.53	0.50	0.34	0.26	0.27	0.36	0.61	2.4	1.9	1.6
Dy (ppm)	1.56	1.97	0.78	2.15	1.45	1.92	1.61	1.10	0.74	0.81	1.42	1.83	8.6	7.2	5.3
Er (ppm)	0.80	0.83	0.39	1.19	0.81	0.99	0.84	0.59	0.42	0.49	0.69	0.99	5.2	4.3	3.1
Yb (ppm)	0.79	1.11	0.46	0.98	0.70	0.97	0.77	0.56	0.35	0.42	0.73	0.96	4.9	4.0	2.9
Mg# in cpx	88.2	80.2	84.5	78.6	81.1	79.6	85.8	89.1	90.4	88.7	88.4	79.5			
XAl _(T) in cpx	0.067	0.052	0.044	0.050	0.057	0.056	0.055	0.061	0.046	0.070	0.049	0.040			
Mg# liq	63.3	48.2	55.6	45.8	49.7	47.3	58.1	65.4	68.3	64.4	63.6	47.1	37.6	45.4	47.2
Nd/Dy(N) liq	2.72	2.73	1.97	2.85	3.30	2.53	2.73	2.41	2.53	2.72	2.35	2.97	2.11	1.83	2.03
Yb/Dy(N) liq	0.77	0.86	0.89	0.70	0.73	0.77	0.73	0.77	0.73	0.78	0.78	0.80	0.85	0.83	0.83

^a u.b. = ultramafic breccia; perid. = peridotite; wehrl. = wehrlite; anort. = anorthosite; troc. = troctolite. Mg# = $100 \times \text{Mg}/(\text{Mg} + \text{Fe}_{\text{tot}})$. Mg# liq is calculated using Fe–Mg K_d of 0.23 [69]. $\text{XAl}_{(T)} = \text{Al}_{(T)}/(\text{Al}_{(T)} + \text{Si})$, where $\text{Al}_{(T)}$ is tetrahedrally coordinated Al. (N) = chondrite normalized concentrations after Sun and McDonough [70]. Partition coefficients from Hart and Dunn [28]. n.d. = not determined.

of 4:1 HF/HClO₄ at 100°C. Rb, Sr, Sm and Nd were separated using established methods at WHOI. Mass spectrometry was carried out at the WHOI using a VG 354 multi collector. NBS 987 and La Jolla standards yielded values of 0.710245–0.710278 (⁸⁷Sr/⁸⁶Sr) and 0.511838–0.511859 (¹⁴³Nd/¹⁴⁴Nd), during the time periods of the measurements.

Helium isotopic compositions were obtained on clean clinopyroxene mineral separates using established methods at WHOI [25]. Because post-intrusion decay of Th and U can lower the initial ³He/⁴He ratios, all of the measurements reported here are obtained by crushing in vacuum, and are assumed to be minimum values for the magmatic ³He/⁴He ratios (Table 2). It is generally accepted that crushing in vacuum selectively releases helium from melt and fluid inclusions within basaltic phenocrysts, which contain the bulk of the magmatic helium, while the radiogenic ⁴He is expected to reside primarily in the matrix [25]. A number of the samples were melted in vacuum, always yielding significantly lower ³He/⁴He ratios, which supports this hypothesis, and also demonstrates that cosmogenic helium is not an important component in these samples.

3. East Greenland gabbros and calculated melt compositions

The layered mafic intrusive rocks of the Kap Edvard Holm (KEH), Nordre Aputiteq, Patulajivit, Kruuse Fjord and Imilik complexes consist mainly of olivine and oxide gabbros, with restricted ranges in mineral compositions [12–15,17,18]. During the evolution of the magma chambers, all were intruded by a primitive melt that crystallized to form wehrlite sills and plugs [12,14,15,26]. The wehrlite intrusions of the KEH are distinct from the host layered gabbros in that the wehrlites are enriched in incompatible elements at a given Mg/Fe of olivine. Hydrous phases such as Ti-amphibole and phlogopite are also abundant in the KEH wehrlites compared to the essentially dry tholeiitic olivine gabbro hosts [12,14,26]. The Lilloise intrusion has a mineralogy similar to the intrusive wehrlites in other plutons, comprising primitive, sometimes amphibole-bearing dunites, wehrlites and pyroxenites as well as subordinate amounts of gabbro [27]. The intrusive wehrlites

of the intrusions south of KEH, all have lower contents of hydrous phases than those at KEH and Lilloise, and have mineral chemistry similar to their host gabbros.

All the analysed clinopyroxene are from cumulates, and since closed-system fractionation can result in considerable fractionation of the REE [14], we have avoided interstitial crystals and rims of cumulus clinopyroxene during the analytical procedure. Equilibrium melt compositions were thus calculated from analyses of clinopyroxene cores [14] (Table 1 and Fig. 2) using experimentally measured crystal/liquid distribution coefficients of Hart and Dunn [28]. The liquid compositions obtained in this way are uncertain given the uncertainties in distribution coefficients, and possible effects of subsolidus redistribution of trace elements. However, since trivalent cations in clinopyroxene diffuse very slowly in low-pressure, sub-solidus conditions [29], REE concentrations are likely to record magmatic compositions. Crystal/liquid distribution coefficients can vary as a function of temperature, pressure and composition. For example, it is evident that REE partitioning between clinopyroxene and liquid is affected by liquid composition [30,31], although ratios of distribution coefficients for different elements tend to be less sensitive to liquid composition. However, for clinopyroxenes with high Ca-Tschermak components, which reflect silica-deficient liquids or high crystallization pressures, the ratio of distribution coefficients for light-REE/heavy-REE changes significantly [31]. In order to investigate this caveat, we can use XAl_(T) as a proxy to the Ca-Tschermak component, and compare clinopyroxenes in our samples to the experimental compositions of Gaetani and Grove [31]. The observed molar proportion of tetrahedral aluminum within our samples from East Greenland, 0.03 to 0.08, is at the low end of the proportion in experimental clinopyroxenes reported by Gaetani and Grove [31]. There is no consistent variation in the REE ratios with respect to XAl_(T) in clinopyroxene in our samples. For instance, clinopyroxenes from the Lilloise intrusion are at one extreme with regard to Yb/Dy and Nd/Dy ratios (Fig. 3), but they also span the entire observed range in XAl_(T) (Table 1). We therefore assume the clinopyroxene/liquid distribution coefficients to be constant for the clinopyroxene compositions reported in this work.

Table 2
Sr, Nd, and He isotope analyses of mineral separates and bulk-rock from 50–47 Ma Tertiary mafic plutons

Location	Sample No.	Rb (ppm)	Sr (ppm)	Nd (ppm)	Sm (ppm)	Rb/Sr	$^{87}\text{Rb}/^{86}\text{Sr}$	$^{87}\text{Sr}/^{86}\text{Sr}_{\text{min}}$	$^{87}\text{Sr}/^{86}\text{Sr}_{\text{f}}$	Sm/Nd	$^{147}\text{Sm}/^{144}\text{Nd}$	$^{143}\text{Nd}/^{144}\text{Nd}_{\text{min}}$	$^{143}\text{Nd}/^{144}\text{Nd}_{\text{f}}$	ϵ_{Nd_i}	^4He (cm^3 STP/g)	$^3\text{He}/^4\text{He}$ (R/R_0)	
Imilik	416705 px	0.12	24.9	1.84	1.05	0.0048	0.01398	0.703392 ± 18	0.703382	0.570	0.3443	0.512489 ± 10	0.512376	-3.72		6.65 ± 0.034	
	416799 px	0.03	21.5	2.30	0.90	0.0014	0.00405	0.703375 ± 17	0.703372	0.392	0.2366	0.512700 ± 40	0.512623	1.09		8.33 ± 0.039	
	416804 pl	1.60	678	1.47	0.20	0.0024	0.00684	0.703381 ± 15	0.703376	0.138	0.0834	0.512648 ± 9	0.512621	1.05			
	416812 pl	1.30	509	3.53	0.80	0.0026	0.00741	0.703415 ± 17	0.703410	0.225	0.1360	0.512670 ± 9	0.512626	1.14			
	416829 px	0.10	22.9	2.84	0.84	0.0044	0.01266	0.703397 ± 19	0.703388	0.294	0.1778	0.512755 ± 9	0.512697	2.53		7.94 ± 0.030	
	416831 pl	2.20	713	3.73	0.83	0.0031	0.00895	0.703392 ± 17	0.703386	0.223	0.1347	0.512797 ± 10	0.512753	3.63			
	312326 pl	2.04	706	4.14	0.69	0.0029	0.00806	0.704323 ± 8	0.704317	0.168	0.1013	0.512773 ± 9	0.512740	3.37			
	312338 blk	3.30	214			0.0154	0.04302	0.704358 ± 8	0.704327								
	312338 pl			1.76	0.24			0.704295 ± 8	0.704317	0.137	0.0827	0.512810 ± 11	0.512783	4.21			
	312383 blk	1.40	600			0.0023	0.00651	0.704418 ± 10	0.704413								
352144 pl	352144 pl	2.13	694	1.75	0.24	0.0031	0.00856	0.704840 ± 15	0.704834	0.061	0.0369	0.512843 ± 8	0.512816	4.87			
	352164 px	0.28	57	6.20	2.10	0.0049	0.01371	0.704345 ± 12	0.704335	0.339	0.2045	0.512841 ± 5	0.512774	4.06			
	1610 px	0.20	49	57.3	2.00	0.0041	0.01139	0.704904 ± 12	0.704896	0.349	0.2108	0.512754 ± 4	0.512685	2.30		9.60 ± 0.045	
	312361 pl	1.20	489	1.88	0.22	0.0025	0.00685	0.704194 ± 14	0.704189	0.117	0.0707	0.512812 ± 13	0.512789	4.33			
Knuse Fjord	71068 pl	0.23	577	0.89	0.06	0.0004	0.00111	0.704039 ± 15	0.704038	0.070	0.0421	0.512511 ± 70	0.512497	-1.36		7.02 ± 0.039	
	Ndr. Aputiteq	3.59	502	5.94	1.65	0.0072	0.02074	0.704083 ± 18	0.704068	0.278	0.1681	0.512882 ± 9	0.512827	5.07			
AP116 blk	AP116 blk	1.41	19.83	4.62		0.0711	0.20620	0.704189 ± 19	0.704043			0.512896 ± 10					
	P78a blk	5.32	737	5.16	1.24	0.0072	0.02093	0.703750 ± 22	0.703735	0.240	0.1448	0.512923 ± 22	0.512876	6.02			
Patulajivit	P97 blk	4.92	345	6.91	1.67	0.0143	0.04136	0.703701 ± 19	0.703672	0.242	0.1459	0.512941 ± 9	0.512893	6.37			
	KIMB12 px	0.73	91	10.70	3.67	0.0081	0.02337	0.703474 ± <10	0.703457	0.343	0.2072	0.512960 ± <10	0.512885	6.21	4.148E-08	7.86 ± 0.157	
Lilloise	73599 px	0.28	50.5	10.96	3.35	0.0055	0.01608	0.703445 ± <10	0.703434	0.306	0.1846	0.512957 ± <10	0.512891	6.31	2.456E-07	7.50 ± 0.036	
	3609 px	0.30	57.6	4.33	1.54	0.0052	0.01510	0.703479 ± <10	0.703468	0.356	0.2148	0.512957 ± <10	0.512880	6.10			
PK504 px	PK504 px	1.60	65	4.78	1.89	0.0246	0.07134	0.704114 ± <10	0.704063	0.395	0.2388	0.512844 ± <10	0.512758	3.73	2.904E-08	10.20 ± 0.100	
	PK504-3 px	0.43	62			0.0069	0.01997	0.703694 ± <10	0.703680			0.512951 ± <10			1.946E-08	10.06 ± 0.102	
3584 px	3584 px	0.30	49	8.02	2.70	0.0061	0.01758	0.703455 ± <10	0.703443	0.337	0.2033	0.512931 ± <10	0.512858	5.67	1.228E-06	10.75 ± 0.075	
	KIMB11 px	0.17	50.7			0.0033	0.00955	0.703427 ± <10	0.703420			0.512967 ± <10			4.779E-07	7.09 ± 0.052	
73504-2 px	73504-2 px	0.25	61.5	0.0040	0.01158			0.704158 ± <10	0.704150			0.512814 ± <10				9.69 ± 0.060	
	73504-1 px							0.703972 ± <10				0.512855 ± <10			2.221E-08	8.90 ± 0.096	
73504-4 px	73504-4 px														2.156E-08	9.03 ± 0.105	
	KIMB2 px														3.626E-07	6.83 ± 0.034	

Suffix to sample numbers refers to analysed material: px = Ca-rich pyroxene; pl = plagioclase; blk = bulk-rock. Concentration of Rb, Sr, Nd and Sm were obtained by isotope dilution mass spectrometry (IDMS), except where numbers are given in *italics*, referring to ion micro-probe analyses. Uncertainties for measured isotopic ratios are presented as 2σ errors in last decimal place. Errors on IDMS is <1% and for ion microprobe analyses <10%. $^{87}\text{Sr}/^{86}\text{Sr}_{\text{min}}$ and $^{143}\text{Nd}/^{144}\text{Nd}_{\text{min}}$ are measured ratios. $^{87}\text{Sr}/^{86}\text{Sr}_{\text{f}}$ and $^{143}\text{Nd}/^{144}\text{Nd}_{\text{f}}$ are calculated initial ratios at 50 Ma.

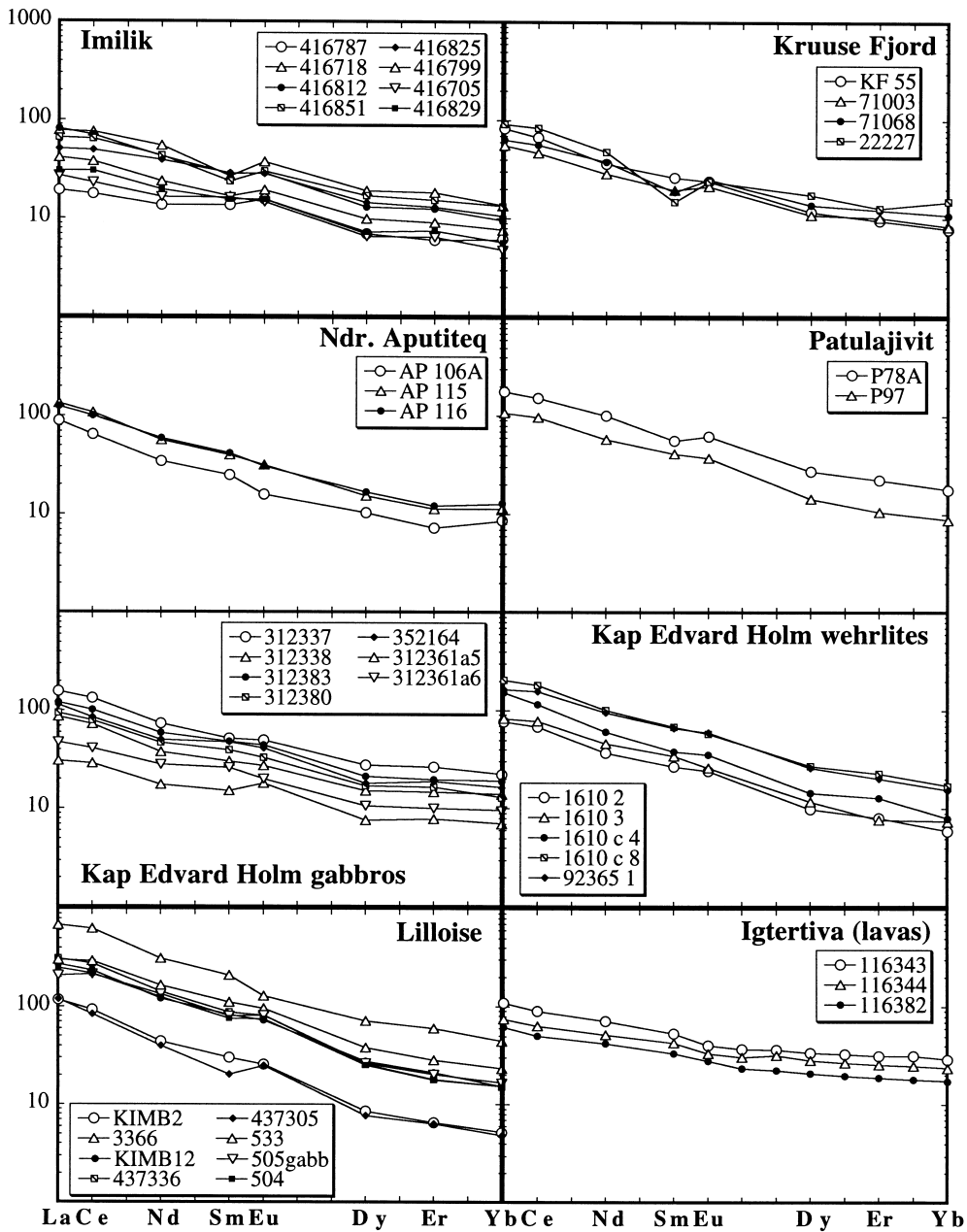


Fig. 2. Rare earth element (REE) profiles of calculated equilibrium liquids based on ion micro-probe analyses of clinopyroxene cores from East Greenland Tertiary mafic intrusions emplaced at 50–47 Ma. (data from Table 1). Also shown are the REE profiles of three basalt flows of the coeval Igtertiva Formation.

The REE composition for calculated liquids of samples from individual intrusions and of the Igtertiva basalts are shown in chondrite normalized fashion in Fig. 2. The calculated liquid composi-

tions in general show smooth patterns, apart from a few anomalies at Sm, which is especially pronounced for two samples from Kruise Fjord, and three samples from Imilik. This feature is unlikely

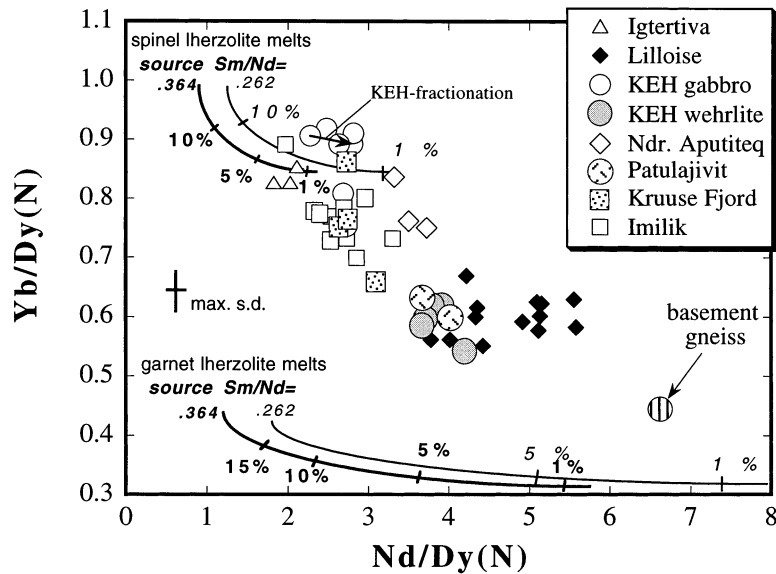


Fig. 3. Calculated liquid compositions of mafic plutons from central East Greenland in terms of their rare earth element characteristics, expressed as LREE to MREE ratio (Nd/Dy(N)) versus HREE to MREE ratio (Yb/Dy(N)). Bars give maximum standard deviation. Basement gneiss composition is from [36]. Arrow 'KEH-fractionation' shows the effect of high-pressure fractionation in the Kap Edvard Holm intrusion [14]. Also given are compositions of aggregate melts generated by fractional melting of a garnet lherzolite and a spinel lherzolite. The melting model is based on the equations for fractional melting given by Gast [59] and Shaw [60]; spinel lherzolite source (ol: 0.46; opx: 0.28; cpx: 0.18; sp: 0.08) and melting modes (ol: -0.44 ; opx: 0.55; cpx: 0.67; sp: 0.22) are from Kelemen et al. [61]. A cpx with 20 mole% wollastonite (Wo) [62] and the normative method of [61] was used to calculate the garnet lherzolite source mode (ol: 0.505; opx: 0.096; cpx: 0.216; gt: 0.183), whereas the melting mode for garnet lherzolite (ol: 0.12; opx: -0.94 ; cpx: 1.37; gt: 0.45) is from Walter and Presnall [63]. REE composition of the model mantle was one of slight LREE depletion with $\text{Nd} = 1.8 \times$ chondrite and $\text{Sm-Yb} = 2 \times$ chondrite [64], which equals $\text{Sm/Nd} = 0.364$ (thick lines). Also shown are melting trajectories for a LREE-enriched mantle with $\text{Nd} = 2.5 \times$ chondrite and $\text{Sm-Yb} = 2 \times$ chondrite, which equals $\text{Sm/Nd} = 0.262$ (thin lines). Distribution coefficients are from Kelemen et al. [65] (ol, opx and spinel) and Shimizu and Kushiro [66] (gt). For cpx in spinel lherzolite the distribution coefficients are from Hart and Dunn [28]. Following the work of McKay et al. [67], who demonstrated a near linear relationship between Wo in cpx and distribution coefficients for the REE, the distribution coefficients for cpx in garnet lherzolite with 20 mole% Wo were calculated by linear interpolation between the Hart and Dunn [28] distribution coefficients (for cpx with 40 mole% Wo) and the opx distribution coefficient data referenced above.

to stem from the employed partition coefficients, and we attribute this phenomenon to an analytical artifact. For samples from the same intrusion, the REE profiles are subparallel, which can be explained in terms of fractional crystallization at low pressure within the magma chamber. The calculated melts from Imilik, Kruse Fjord, Nordre Aputiteq and Kap Edvard Holm gabbros are similar to the basalts from Igtertiva in having relatively unfractionated REE ratios. Samples from Lilloise, Patulajivit and Kap Edvard Holm wehrlites have steeper REE profiles, not only at the light to middle REE range, but also for the middle to heavy REE range. These features are illustrated by REE ratios in Fig. 3, where the x -axis is Nd/Dy(N) , a ratio of light- to middle-

REE where (N) denotes chondrite-normalized ratios, and the y -axis is Yb/Dy(N) , a ratio of heavy- to middle-REE. Thus, data in the right-hand side of the diagram are light-REE enriched, and those plotting towards low Yb/Dy(N) ratios are heavy-REE depleted. Significant fractionation of REE can result from fractional crystallization at elevated pressures where clinopyroxene or even garnet becomes important in the fractionating assemblage [14,32–35]. A suite of gabbros from the Kap Edvard Holm intrusion have been demonstrated to be related through fractional crystallization at elevated pressures [14], as shown with a vector 'KEH-fractionation' in Fig. 3. Within all other intrusions, REE ratios show no correlation with Mg# of the analysed clinopyroxene,

suggesting that fractional crystallization has played a minor role in creating their REE variation. Due to the highly diverse lithology of Lilloise rocks [27], we are, however, uncertain whether the large variation in Nd/Dy(N) for Lilloise calculated liquids (Fig. 3) can be attributed to primary melt characters or rather is a result of crystal fractionation and melt-rock reaction processes within the intrusion.

4. Sr and Nd isotopic compositions

Before discussing mantle melting processes, we first evaluate the alternative hypothesis that the trends defined by melts from the gabbro pluton in Fig. 3 are the result of contamination of mantle melts generated in the spinel stability field, with material from Archaean gneisses that host the intrusions, and which is enriched in LREE and MREE. In Fig. 3 is shown the composition of a typical Archaean basement gneiss [36]. Although Fig. 3 may suggest that the range in the REE ratios defined by the gabbro melts reflect a varying degree of contamination of melt from a spinel peridotite with such gneissic material, the Nd isotopic composition of the gabbros appears to argue against this. In Fig. 4 we show the variation in ϵ_{Nd} of the gabbro samples against the REE ratios of their calculated liquids. Also shown is the composition of a melt produced by 5% partial melting of a spinel peridotite with an ϵ_{Nd} of +6, similar to the more radiogenic gabbro samples (5% is arbitrarily chosen; melting parameters described in caption to Fig. 3). The curves give the composition of hybrid melts produced by bulk assimilation of a granulite facies gneiss from SE Greenland [37]. We want to stress that the actual contamination process envisioned is of less importance, since we are mainly interested in the influence on the REE ratios. For instance, more realistic processes, involving selective contamination (e.g. [38]) and coupled assimilation and fractional crystallization (e.g. [39]) would result in greatly magnified negative ϵ_{Nd} values for the contaminated melts with only less effect on the REE ratios. Since isotopic exchange between two reservoirs is at least an order of magnitude faster than the equilibration of concentrations [40] simple bulk assimilation can be regarded as a 'worst case' setting for the influence of contamination on the REE

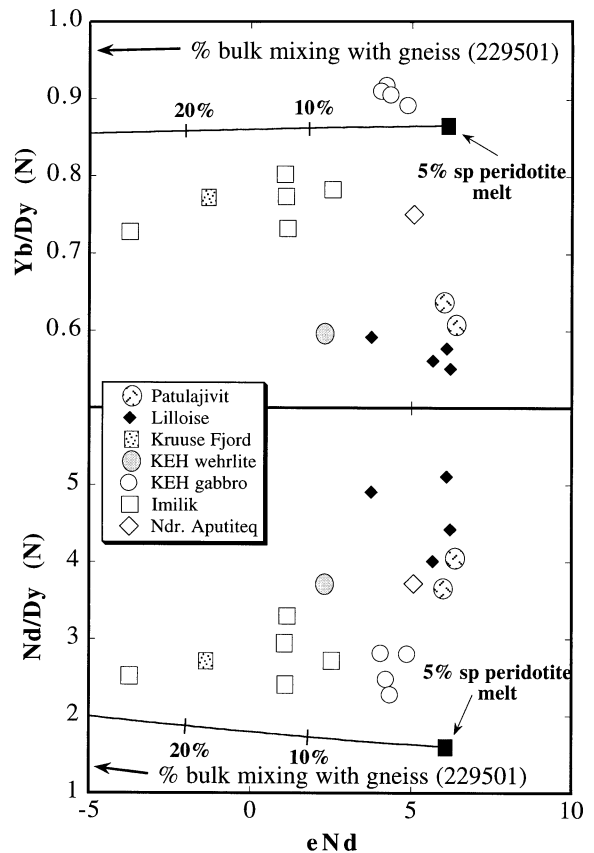


Fig. 4. Neodymium isotopic composition for the Tertiary gabbros, as determined on plagioclase and clinopyroxene mineral separates and whole rock samples (Table 2), against REE ratios of calculated liquids. Also shown are compositions of hypothetical liquids produced by bulk assimilation of a 5% spinel peridotite melt with an ϵ_{Nd} of +6, with a granulite facies gneiss #229501 from Taylor et al. [37]. While the trend towards lower ϵ_{Nd} for the Imilik gabbros qualitatively can be explained in terms of crustal contamination, the diagram shows that this process does not alter the REE ratios significantly in this range of ϵ_{Nd} .

characteristics of the gabbro melts. It is therefore implausible that the range of REE ratios in the gabbro melts stems from assimilation of crustal material.

Combined Sr and Nd isotopic compositions (Fig. 5) shows two trends that require at least two contamination components. One with a distinct radiogenic Sr isotopic composition, and one with a distinct unradiogenic Nd and Sr isotopic composition. As also shown in Fig. 4, the trend towards unradiogenic Nd (and Sr) isotopic composition is

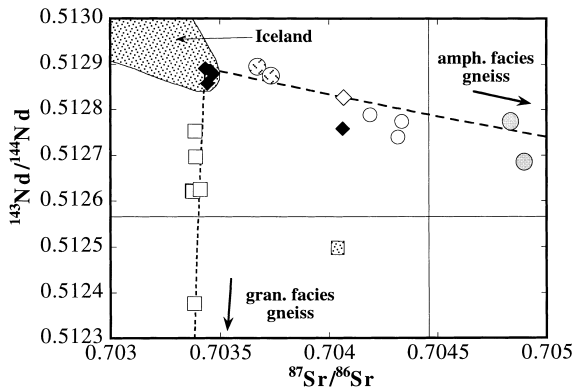


Fig. 5. Combined Sr and Nd isotope compositions for the Tertiary gabbros corrected for decay of Rb and Sm over 50 my. Symbols as in Figs. 3 and 4. The data forms two trends; one towards high $^{87}\text{Sr}/^{86}\text{Sr}$, and one towards low $^{143}\text{Nd}/^{144}\text{Nd}$ and low $^{87}\text{Sr}/^{86}\text{Sr}$. Lilloise rocks define the high $^{143}\text{Nd}/^{144}\text{Nd}$, low $^{87}\text{Sr}/^{86}\text{Sr}$ focal point. The two trends suggest contribution from old amphibolite and granulite facies gneisses, respectively. The end-member compositions are #229501 [37] for the granulite facies gneiss, and #CL87-5217 [38] for the amphibolite facies gneiss. A calculated melt from the Lilloise intrusion was taken as the uncontaminated end member. Note that the uncontaminated Lilloise samples all fall at the low $^{143}\text{Nd}/^{144}\text{Nd}$ and high $^{87}\text{Sr}/^{86}\text{Sr}$ end of the Iceland compositional field. Iceland data from Hémond et al. [50].

consistent with assimilation of Archaean basement material in granulite facies. The high $^{87}\text{Sr}/^{86}\text{Sr}$ component may be represented by an amphibolite facies basement gneiss from East Greenland [38]. The Lilloise samples thus appear to form the group of least contaminated melts in the sample collection, and we note that they, in terms of Sr and Nd isotopic composition, are similar to the high $^{87}\text{Sr}/^{86}\text{Sr}$, low $^{143}\text{Nd}/^{144}\text{Nd}$ end of the Iceland compositional field.

5. Mantle melting processes

Melt trajectories for partial fusion of spinel- and garnet-bearing lherzolites are shown in Fig. 3 (thick lines; see figure caption for details). The REE profile of the model lherzolite mantle source is one of slight LREE depletion (Sm/Nd of 0.364), which is suggested by the positive ϵ_{Nd} isotopic composition of the uncontaminated samples of mainly the Lilloise intrusion. Pooling of melts generated in garnet- and spinel-peridotites will result in linear trends in Fig. 3

because of the common denominator on the two axes. Calculated liquids in equilibrium with clinopyroxene from all studied intrusions have $\text{Nd}/\text{Dy}(\text{N})$ greater than 2.0. This is striking because liquids produced by more than a few percent partial melting of primitive mantle in spinel lherzolite facies have $\text{Nd}/\text{Dy}(\text{N})$ lower than 2 (Fig. 3). Additionally, the compositional fields of all of the intrusions extend to much lower $\text{Yb}/\text{Dy}(\text{N})$ than melts from spinel lherzolite. Because of the strong fractionation of REE in garnet (in which Yb is highly compatible, Dy is compatible, and Nd is incompatible), these data suggest that garnet was a residual phase in the source of the liquids parental to these intrusions. This would entail initial melting at pressures in excess of about 25 kbar, where garnet is stable at magmatic temperatures in mantle peridotite [41].

Aggregation of LREE-enriched, HREE-depleted melt increments from garnet lherzolite with LREE-depleted melt increments from spinel lherzolite may thus be a viable explanation for the array of compositions of the 50–47 Ma melts outlined in Fig. 3. However, the compositional array is displaced to higher $\text{Nd}/\text{Dy}(\text{N})$ values than can be produced by melting of a LREE-depleted lherzolite. The low $\text{Yb}/\text{Dy}(\text{N})$ end of the gabbro melt field in Fig. 3 suggests that the garnet lherzolite melt component must have had $\text{Nd}/\text{Dy}(\text{N})$ somewhat higher than 5.8, which is the maximum value for a minute melt fraction with the given parameters listed in the caption to Fig. 3. Similarly, the high $\text{Yb}/\text{Dy}(\text{N})$ end of the gabbro melt field requires the spinel melt component to have $\text{Nd}/\text{Dy}(\text{N})$ higher than 2.3. This suggests that the mantle source must have been LREE enriched. Assuming a mantle lherzolite with a flat REE profile ($\text{Sm}/\text{Nd} = 0.322$) only results in a modest increase in $\text{Nd}/\text{Dy}(\text{N})$ for melts generated in both garnet and spinel pressure ranges. In Fig. 3 is shown the melting trajectories of a LREE-enriched lherzolite, with $\text{Sm}/\text{Nd} = 0.262$ (thin lines). The gabbro melt field then lies within what can be produced by relatively small degree melting of LREE-enriched garnet and spinel lherzolite (1–5% and 1–10%, respectively).

Based on the REE systematics, we therefore conclude that the mantle source of the gabbro melts was LREE enriched, and that the gabbro melts were generated by decompression melting of ascending mantle, which crossed the solidus in the shallow-

est part of the garnet stability field, producing only 1–5% melt before transformation into spinel peridotite took place (see e.g. [42]). Continued melting of the spinel peridotite produced the high Yb/Dy, low Nd/Dy end member in our data set, and the trend of the data toward lower Yb/Dy and higher Nd/Dy reflects the additional presence of varying proportions of high pressure melts. It is notable, that the lower-right end of the data array in Fig. 3 is restricted to the intrusions occurring around 67–68°N (i.e. Lilloise, KEH wehrlite, Patulajivit) whereas the upper-left end of the data array is made up by gabbros and lavas from the entire study area between 66°N and 70°N (KEH and Imilik gabbros, Igtertiva Formation basalts). We therefore suggest that the proportion of melts from a garnet-bearing source was higher beneath the Patulajivit–Lilloise sector than in the remaining part of the East Greenland Tertiary Igneous Province at 50–47 Ma.

6. Helium isotopes and the enriched mantle component

Preliminary He isotope data shown in Fig. 6, demonstrate that samples from the Lilloise and KEH wehrlites have $^3\text{He}/^4\text{He}$ ratios significantly higher than present day MORB. This points towards a relatively undegassed lower mantle component in the source of these rocks as suggested for, e.g., Icelandic, Hawaiian, and Samoan basalts [25,43,44]. Four samples of ultramafic intrusives from Imilik and Kruise Fjord show lower $^3\text{He}/^4\text{He}$ isotopic ratios. Note that all our $^3\text{He}/^4\text{He}$ values represent minimum values for the parental magma, since all of the rock samples have been affected by about 50 million years of ^4He ingrowth due to radioactive decay of U and Th. Along this line, the large range of $^3\text{He}/^4\text{He}$ ratios found in Lilloise clinopyroxenes may be due in part to the presence of post-intrusion, radiogenic helium.

The unradiogenic He isotope character of many hotspots is linked to the existence of upwelling, anomalously hot lower mantle material [45], that causes melting to initiate at higher pressures than the surrounding upper mantle material [46,47]. In this view, the samples of the 50–47 Ma gabbros with the highest $^3\text{He}/^4\text{He}$ and lowest Yb/Dy(N) represent melts with the highest proportion of the plume com-

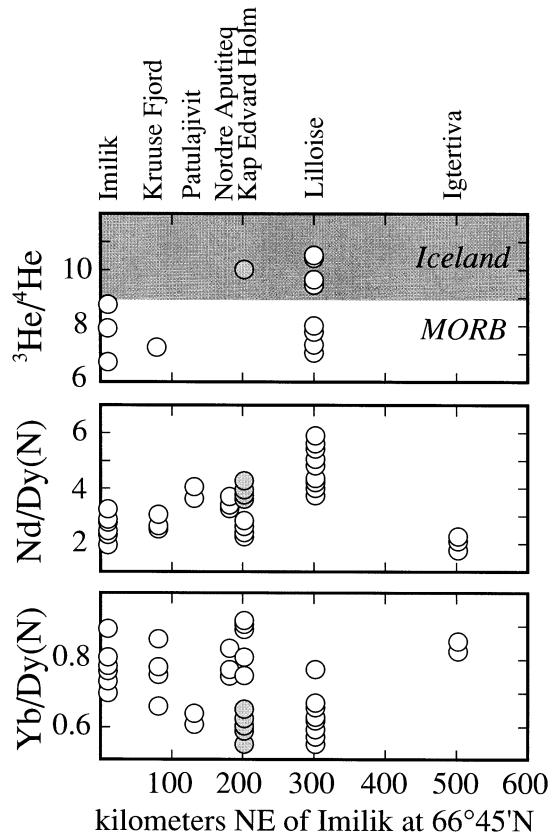


Fig. 6. Summary of geochemical data for 50–47 Ma magmatic rocks along the coast of East Greenland, arranged in order of distance north of the Imilik intrusion at about 67°N. REE data, for calculated liquids, are from our data in Table 1. He data are from our data in Table 2. Calculated liquids from 200 to 300 km north of Imilik have the strongest signature of small degrees of melting in the presence of garnet (light-REE enrichment, heavy-REE depletion, and are most similar in their He isotopic characteristics to lavas erupted in present day Iceland (gray field). The KEH wehrlites are illustrated with filled circles to distinguish them from the KEH gabbros.

ponent. An explanation for the spatial distribution of chemical and isotopic characteristics as depicted in Fig. 6, could be the presence of the Icelandic mantle plume, approaching the present day coast line at about 69°N several million years after the initiation of sea-floor spreading to the east [1,2,48,49].

As noted above, the Sr–Nd isotopic composition of samples from the Lilloise intrusion plot at the high $^{87}\text{Sr}/^{86}\text{Sr}$, low $^{143}\text{Nd}/^{144}\text{Nd}$ end of the field defined by Icelandic lavas (Fig. 5). The convergence at the

Lilloise samples of the two arrays towards amphibolite and granulite facies crustal material, respectively, suggests that the Lilloise samples may represent the isotopic composition of uncontaminated melts for all gabbros. The Iceland compositional field itself can be interpreted as representing mixing of melts from two mantle sources: (1) a MORB type mantle, that isotopically lies at the low $^{87}\text{Sr}/^{86}\text{Sr}$, high $^{143}\text{Nd}/^{144}\text{Nd}$ end of the Iceland field, and (2) a LREE-enriched mantle defining the high $^{87}\text{Sr}/^{86}\text{Sr}$, low $^{143}\text{Nd}/^{144}\text{Nd}$ end of the Iceland field [50]. The LREE-enriched mantle appears to be an intrinsic feature of the Iceland mantle plume, and has likewise been argued for the early pre-breakup volcanics in East Greenland by Fram and Lesher [35]. We note that the LREE enrichment of the mantle source for the gabbro melts expressed by the Sm/Nd of 0.262 (see above Section 5) is similar to the value of 0.25 suggested for the plume component in the Iceland hot spot by Fram and Lesher [35]. Since there is no isotopic or trace-element evidence for an involvement of the MORB type mantle in the generation of the 50–47 Ma gabbros, we conclude on the basis of the available data that the mantle source for the post-breakup volcanism along the East Greenland margin was the plume component of the Iceland hot spot.

7. Regional perspective

Precise $^{40}\text{Ar}/^{39}\text{Ar}$ geochronology suggests that basaltic volcanism along the East Greenland rifted margin occurred in three discrete time windows as discussed in detail in Ref. [1]. Briefly, magmatism began with the eruption of the Lower Lava Series from ODP Leg 152 at 63°N, Site 917 (63–61 Ma [51]), and with the Lower Lava Series and related dykes (>56 Ma [9,52]) in the Patulajivit–Lilloise sector. The major expression of flood basalt magmatism that formed the Blosseville–Scoresby Sund plateau basalts (Middle Series) at 56–55 Ma; [8–10], was contemporaneous with the formation of seaward-dipping reflector sequences, such as the Upper Series of ODP 63°N transect, Site 917 [53], the basalts of the Vøring Plateau [54] and was roughly coeval with the establishment of the oceanic spreading ridge offshore [11]. The 50–47 Ma gabbroic intrusions along the central East Greenland coast, the

Igtertiva Formation lavas at Kap Dalton [7,9,21] and some coast parallel dykes of transitional affinity [23] mark the termination of main tholeiitic volcanism on the continental margin.

The REE systematics of these stages of rift magmatism are presented in Fig. 7 for comparison. The pre-breakup event was dominated by relatively high pressure melts, with the top of the melting column in the spinel stability field. Compared to this first melting event, basalts from breakup around 56 Ma are displaced towards higher Yb/Dy (N), which would imply increasing proportions of melts from the low-pressure (spinel stability) melting region, and thereby a decreasing mean pressure of melting. Also, their slightly steeper trends in Fig. 7, relative to pre-breakup basalts, would suggest increasing mean degrees of melting. This evolution to higher degrees of melting at lower average pressure has been well established by the modeling of Fram and Lesher [35,55], who ascribed it to decreasing lithosphere thickness during rifting, also described as the ‘lid effect’ by Ellam [56].

The late basaltic volcanism at around 50–47 Ma, which postdates the initiation of oceanic crust formation at anomaly 24R by 5–9 Ma, is chemically very distinct from the earlier volcanic products. First, the high Nd/Dy for the post-breakup melts appears to require a LREE enrichment of the mantle source. Because of the positive ϵ_{Nd} for the uncontaminated melts, this enrichment must have been a recent event. Second, the generally lower mean degree of melting, and the relatively small degree of melting within the low-pressure, spinel stability field (inferred from Fig. 3), suggest a more restricted vertical extent of the melting column at this stage of evolution of the continental margin. An interpretation of this behavior could be that residual mantle, depleted during the breakup phase, was added to the lithosphere due to the relative buoyancy of high Mg# residues [57]. Combined with extensive amounts of underplated, igneous material generated during flood basalt magmatism, the addition of depleted mantle to the lithosphere resulted in a significant thickening of the plate (the ‘lid’) at the continental margin after breakup. This restricted the minimum pressure of melting of upwelling asthenospheric mantle; in other words ‘putting the lid back on top’ of the melting column at the continental margin.

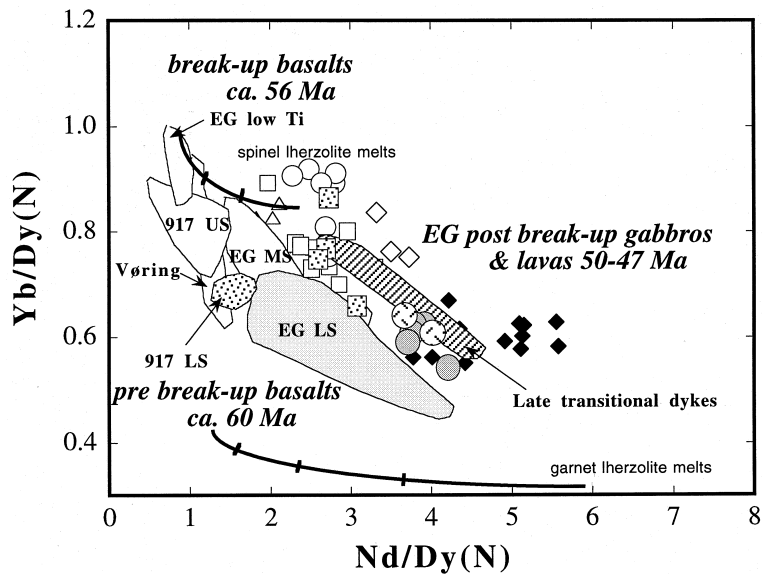


Fig. 7. Compositional variation of basaltic melts from the initial stages of North Atlantic magmatism. Melting trajectories for garnet and spinel lherzolites as in Fig. 3. The ca. 60 Ma pre-breakup basalts (stippled patterns) all have a strong garnet signature (HREE depletion) and low amounts of melting at low pressures (thick lithosphere as suggested by Fram and Leshar [55]). At the time of establishment of an ocean spreading ridge (continental breakup, unfilled patterns) at 56 Ma, melting still took place in the garnet stability field, but with extensive degrees of melting also at lower pressures in the spinel stability field [55]. The strongly LREE-enriched basaltic melts at 50–47 Ma expressed by the gabbro intrusions, the Igtertiva Formation and late coast-parallel, transitional dykes (post-breakup, hatched patterns) reflect mantle melting at predominantly high pressures. Data from [35] (East Greenland lower lavas); [42,68] (Leg 152 Site 917, Lower and Upper Series); [54] (Vøring Plateau); [DLC; unpublished data] (East Greenland main lavas; EG ML and EG low Ti) and [23] (late coast parallel dykes).

From the available data, the 50–47 Ma post-breakup volcanic episode appears to be confined to a coastal region of approximately 600 km between 66° and 70°N, and is absent from the continent–ocean transition zone 200 km further to the south, as sampled by the ODP Leg 152 [53]. The strongest plume signature appears to be concentrated within a narrow zone about 150 km wide, from the Lilloise intrusion in the north, through the KEH wehrlites, to the Patulajivit gabbros in the south (Figs. 1, 3 and 6). One may find the explanation for this in elevated mantle potential temperatures beneath this portion of the margin during the passage of the Iceland mantle plume, coupled with greater lithospheric thickness resulting from the vigorous magmatism at breakup. The spatial distribution of the 50–47 Ma magmatism onshore further correlates with the bathymetry of the Greenland–Iceland Rise, which is the offshore result of excess magmatism above the Iceland mantle plume [58]. The persistence of basaltic magmatism at the continental margin 5–9 Ma after the estab-

lishment of an oceanic spreading ridge may thus be understood in terms of the increasing proximity of the Icelandic mantle plume to the East Greenland coastline (see [1] for detailed discussion). Such a model would be in accordance with the interpretation of plate reconstruction by Morgan [2], Duncan and Richards [49], and Lawver and Muller [48] of the Iceland plume track. Continuing sampling of offshore basalts in the Denmark Strait by the DLC (scheduled 1998) will help to constrain whether the post-breakup basaltic magmatism was confined to the East Greenland continental margin, or was involved in the build-up of the thick oceanic crust of the Greenland–Iceland Rise.

Acknowledgements

Thanks for assistance in the field to Dennis Bird, Nick Rose, Geoff Radford, Andy Tuthill, Bob Gannicott, Bill Mosher, Guy Della Valle, Göran Lindmark,

John Arnason, Troels Nielsen, and Craig Manning. Dennis Bird kindly gave access to samples of gabbros from Patulajivit and Nordre Aputiteq. Thanks also to Stuart Watt and Lotte Melchior Larsen for identifying samples from the Igtertiva Formation for analyses, and to Stan Hart for access to the clean lab facilities at WHOI. This manuscript has benefited from discussions with Chip Lesher, Hans Christian Larsen, Lotte Melchior Larsen, Troels Nielsen, Michael Storey, Karen Hanghøj Sørensen, Ole Stecher, and Karl Pivat. Constructive reviews by N.T. Arndt; M. Dungan; G. Fitton and C.E. Lesher are greatly appreciated and improved the quality of this paper substantially. This study was supported by The Danish National Research Foundation. [FA]

References

- [1] C. Tegner, R.A. Duncan, S. Bernstein, C.K. Brooks, D.K. Bird, M. Storey, ^{40}Ar – ^{39}Ar geochronology of Tertiary mafic intrusions along the East Greenland rifted margin: relation to flood basalts and the Iceland hotspot track, *Earth Planet. Sci. Lett.* 156 (1998) 75–88.
- [2] W.J. Morgan, Plate motions and deep mantle convection, *Geol. Soc. Am. Mem.* 132 (1972) 7–10.
- [3] C.K. Brooks, Rifting and doming in southern East Greenland, *Nature* 244 (1973) 23–25.
- [4] C.K. Brooks, T.D.F. Nielsen, T.S. Petersen, The Blosseville Coast basalts of East Greenland: their occurrence, composition, and temporal variations, *Contrib. Mineral. Petrol.* 58 (1976) 279–292.
- [5] L.M. Larsen, W.S. Watt, Episodic volcanism during break-up of the North Atlantic: evidence from the East Greenland plateau basalts, *Earth Planet. Sci. Lett.* 73 (1985) 105–116.
- [6] R.H. Noble, R.M. Macintyre, P.E. Brown, Age constraints on Atlantic evolution: timing of magmatic activity along the E Greenland continental margin, in: Morton, A.C., Parson, L.M. (Eds.), *Early Tertiary Volcanism and the Opening of the NE Atlantic*, *Spec. Publ. Geol. Soc.* 39 (1988) 201–214.
- [7] L.M. Larsen, W.S. Watt, M. Watt, Geology and petrology of the Lower Tertiary plateau basalts of the Scoresby Sund region, East Greenland, *Geol. Surv. Greenl. Bull.* 157 (1989) 1–164.
- [8] H. Hansen, D.C. Rex, P.G. Guise, C.K. Brooks, $^{40}\text{Ar}/^{39}\text{Ar}$ ages on early Tertiary basalts from the Scoresby Sund area, East Greenland, *Newslett. Stratigr.* 32 (1995) 103–116.
- [9] M. Storey, R.A. Duncan, H.C. Larsen, R. Waagstein, L.M. Larsen, C. Tegner, C.E. Lesher, Impact and Rapid flow of the Iceland plume beneath Greenland at 61 Ma, *EOS Trans. Am. Geophys. Union* 77 (1996) F839.
- [10] A.K. Pedersen, M. Watt, W.S. Watt, L.M. Larsen, Structure and stratigraphy of the Early Tertiary basalts of the Blosseville Kyst, East Greenland, *J. Geol. Soc. London* 154 (1997) 565–570.
- [11] H.C. Larsen, A multiple and propagating rift model for the NE Atlantic, in: Morton, A.C., Parson, L.M. (Eds.), *Early Tertiary Volcanism and the Opening of the NE Atlantic*, *Publ. Geol. Soc.* 39 (1988) 157–158.
- [12] S. Bernstein, M.T. Rosing, C.K. Brooks, D.K. Bird, An ocean-ridge type magma chamber at a passive volcanic, continental margin: the Kap Edvard Holm layered gabbro complex, East Greenland, *Geol. Mag.* 129 (1992) 437–456.
- [13] C. Tegner, J.R. Wilson, C.K. Brooks, Intraplutonic quench zones in the Kap Edvard Holm layered gabbro complex, East Greenland, *J. Petrol.* 34 (1993) 681–710.
- [14] S. Bernstein, P.B. Kelemen, C.K. Brooks, Evolution of the Kap Edvard Holm Complex: a mafic intrusion at a rifted continental margin, *J. Petrol.* 37 (1996) 497–519.
- [15] J.G. Arnason, D.K. Bird, S. Bernstein, N.M. Rose, C.E. Manning, Petrology and geochemistry of the Kruuse Fjord Gabbro Complex, East Greenland, *Geol. Mag.* 134 (1997) 67–89.
- [16] L.R. Wager, Geological investigations in East Greenland, Part IV: The stratigraphy and tectonics of Knud Rasmussens Land and the Kangerdlugssuaq region, *Meddr. Grønland* 134 (1947) 1–64.
- [17] C.K. Brooks, T.F.D. Nielsen, The Phanerozoic development of the Kangerdlugssuaq area, East Greenland, *Meddr. Grønland* 9 (1982) 3–30.
- [18] D.K. Bird, C.E. Manning, N.M. Rose, Hydrothermal alteration of Tertiary layered gabbros, East Greenland, *Am. J. Sci.* 288 (1988) 405–457.
- [19] J.S. Myers, Structure of the coastal dyke swarm and associated plutonic intrusions of East Greenland, *Earth Planet. Sci. Lett.* 46 (1980) 407–418.
- [20] R.J. Neve, M.E. Brandriss, D.K. Bird, M.O. McWilliams, J.R. O'Neill, Tertiary plutons monitor climate change in East Greenland, *Geology* 22 (1994) 775–778.
- [21] W.S. Watt, L.M. Larsen, M. Watt, Volcanic history of the Lower Tertiary plateau basalts in the Scoresby Sund region, East Greenland, *Rapp. Grøn. Geol. Unders.* 128 (1986) 147–156.
- [22] T.F.D. Nielsen, The Tertiary dike swarms of the Kangerdlugssuaq area, East Greenland, *Contrib. Mineral. Petrol.* 67 (1978) 63–78.
- [23] K. Hanghøj, Geochemistry of the East Greenland Tertiary dyke swarm; temporal and spatial variations. Ph.D. Thesis, University of Copenhagen, 1998, 123 pp.
- [24] N. Shimizu, M.P. Semet, C.J. Allegre, Geochemical applications of quantitative ion-microprobe analysis, *Geochim. Cosmochim. Acta* 42 (1978) 1321–1334.
- [25] M.D. Kurz, T.C. Kenna, J.C. Lassiter, D.J. DePaolo, Helium isotopic evolution of Mauna Kea Volcano: First results from the 1 km drill core, *J. Geophys. Res.* 101 (1996) 11781–11791.
- [26] C. Tegner, J.R. Wilson, A late ultramafic suite in the Kap Edvard Holm layered gabbro complex, East Greenland, *Geol. Mag.* 130 (1993) 431–442.
- [27] A.D. Chambers, P.E. Brown, The Lilloise Intrusion, East

- Greenland: fractionation of a hydrous alkali picritic magma, *J. Petrol.* 36 (1995) 933–963.
- [28] S.R. Hart, T. Dunn, Experimental cpx/melt partitioning of 24 trace elements, *Contrib. Mineral. Petrol.* 113 (1993) 1–8.
- [29] R. Freer, Diffusion in silicate minerals and glasses: A data digest and guide to the literature, *Contrib. Mineral. Petrol.* 76 (1981) 440–454.
- [30] W.E. Gallahan, R.L. Nielsen, The partitioning of Sc, Y, and the rare earth elements between high-Ca pyroxene and natural mafic to intermediate lavas at 1 atmosphere, *Geochim. Cosmochim. Acta* 56 (1992) 2387–2404.
- [31] G.A. Gaetani, T.L. Grove, Partitioning of rare earth elements between clinopyroxene and silicate melt: crystal-chemical controls, *Geochim. Cosmochim. Acta* 59 (1995) 1951–1962.
- [32] F. Albarède, V. Tamagnan, Modelling the recent geochemical evolution of the Piton de la Fournaise Volcano, Réunion Island, 1931–1986, *J. Petrol.* 29 (1988) 997–1030.
- [33] S. Bernstein, High-pressure fractionation in rift-related basaltic magmatism: Faeroe plateau basalts, *Geology* 22 (1994) 815–818.
- [34] S. Bernstein, High-pressure fractionation in rift-related basaltic magmatism: Faeroe plateau basalts, Reply to Comment by Kerr, A.C. and Thompson, R.N., *Geology* 23 (1995) 672.
- [35] M.S. Fram, C.E. Lesher, Generation and polybaric differentiation of East Greenland early Tertiary flood basalts, *J. Petrol.* 38 (1997) 231–275.
- [36] B.L. Weaver, J. Tarney, Lewisian gneiss geochemistry and Archaean crustal development models, *Earth Planet. Sci. Lett.* 55 (1981) 171–180.
- [37] P.N. Taylor, F. Kalsbeek, D. Bridgwater, Discrepancies between neodymium, lead and strontium model ages from the Precambrian of southern East Greenland: evidence for a Proterozoic granulite-facies event affecting Archaean gneisses, *Chem. Geol.* 94 (1992) 281–291.
- [38] J. Blichert-Toft, C.E. Lesher, M.T. Rosing, Selectively contaminated magmas of the Tertiary East Greenland macrodike complex, *Contrib. Mineral. Petrol.* 110 (1992) 154–172.
- [39] D.J. DePaolo, Trace element and isotopic effects of combined wallrock assimilation and fractional crystallization, *Earth Planet. Sci. Lett.* 53 (1981) 189–202.
- [40] C.E. Lesher, Decoupling of chemical and isotopic exchange during magma mixing, *Nature* 344 (1990) 235–237.
- [41] H.S.C. O'Neill, The transition between spinel lherzolite and garnet lherzolite, and its use as a geobarometer, *Contrib. Mineral. Petrol.* 77 (1981) 185–194.
- [42] M.S. Fram, C.E. Lesher and A.M. Volpe, Mantle melting systematics: transition from continental to oceanic volcanism on the Southeast Greenland margin, in: Saunders, A.D., Larsen, H.C., Clift, P.D., Wise, S. (Eds.), *Proc. ODP Sci. Res. 152. Ocean Drilling Program, College Station, TX, 1998*, in press.
- [43] M.D. Kurz, P.S. Meyer, H. Sigurdsson, Helium isotope systematics within the neovolcanic zones of Iceland, *Earth Planet. Sci. Lett.* 74 (1985) 291–305.
- [44] K.A. Farley, H. Craig, Mantle plumes and mantle sources, *Science* 258 (1992) 821–822.
- [45] M.D. Kurz, Mantle heterogeneity beneath oceanic islands: some inferences from isotopes, *Philos. Trans. R. Soc. London Ser. A* 342 (1993) 91–103.
- [46] E. Klein, C.H. Langmuir, Global correlations of ocean ridge basalt chemistry with axial depth and crustal thickness, *J. Geophys. Res.* 92 (1987) 8089–8115.
- [47] D. McKenzie, M.J. Bickle, The volume and composition of melt generated by extension of the lithosphere, *J. Petrol.* 29 (1988) 625–679.
- [48] L.A. Lawver, R.D. Muller, Iceland hotspot track, *Geology* 22 (1994) 311–314.
- [49] R.A. Duncan, M.A. Richards, Hotspots, mantle plumes, flood basalts, and true polar wander, *Rev. Geophys.* 29 (1991) 31–50.
- [50] C. Hémond, N.T. Amdt, U. Lichtenstein, A.W. Hofmann, N. Oskarsson, S. Steinthorson, The heterogeneous Iceland plume: Nd–Sr–O isotopes and trace element constraints, *J. Geophys. Res.* 98 (1993) 15833–15850.
- [51] C.W. Sinton and R.A. Duncan, ^{40}Ar – ^{39}Ar ages of lavas from the southeast Greenland Margin, ODP Leg 152 and the Rockall Plateau, DSDP Leg 81, in: Saunders, A.D., Larsen, H.C., Clift P.D., Wise, S. (Eds.), *Proc. ODP Sci. Res. 152. Ocean Drilling Program, College Station, TX, 1998*, in press.
- [52] T.F.D. Nielsen, N.J. Soper, C.K. Brooks, A.M. Faller, A.C. Higgins, D.W. Matthews, The pre-basaltic sediments and the Lower Basalts at Kangerdlugssuaq, East Greenland: their stratigraphy, lithology, palaeomagnetism and petrology, *Meddr. Grønland Geosci.* 6 (1981) 3–25.
- [53] H.C. Larsen and A.D. Saunders, Tectonism and volcanism at the southeast Greenland rifted margin: A record of plume impact and later continental rapture, in: Saunders, A.D., Larsen, H.C., Clift, P.D., Wise, S. (Eds.), *Proc. ODP Sci. Res. 152. Ocean Drilling Program, College Station, TX, 1998*, in press.
- [54] L.G. Viereck, J. Hertogen, L.M. Parson, A.C. Morton, D. Love and I.L. Gibson, Chemical stratigraphy and petrology of the Vøring plateau tholeiitic lavas and intermediate volcanoclastic sediments at ODP Hole 642E, in: Eldholm, O., Thiede J., Taylor, E. (Eds.), *Proc. ODP Sci. Res. 642. Ocean Drilling Program, College Station, TX, 104 (1989) 367–396*,
- [55] M.S. Fram, C.E. Lesher, Geochemical constraints on mantle melting during creation of the North Atlantic basin, *Nature* 363 (1993) 712–715.
- [56] R.M. Ellam, Lithospheric thickness as a control on basalt geochemistry, *Geology* 20 (1992) 153–156.
- [57] T.H. Jordan, Composition and development of the continental tectosphere, *Nature* 274 (1978) 544–548.
- [58] G.E. Vink, A hotspot model for Iceland and the Vøring Plateau, *J. Geophys. Res.* 87 (1984) 10677–10688.
- [59] P.W. Gast, Trace element fractionation and the origin of tholeiitic and alkaline magma types, *Geochim. Cosmochim. Acta* 32 (1968) 1057–1086.

- [60] D.M. Shaw, Trace element fractionation during anatexis, *Geochim. Cosmochim. Acta* 34 (1970) 237–243.
- [61] P.B. Kelemen, H.J.B. Dick, J.E. Quick, Formation of harzburgite by pervasive melt/rock reaction in the upper mantle, *Nature* 358 (1992) 635–641.
- [62] J. Longhi, Liquidus equilibria of some primary lunar and terrestrial melts in the garnet stability field, *Geochim. Cosmochim. Acta* 59 (1995) 2375–2386.
- [63] M.J. Walter, D.C. Presnall, Melting behaviour of simplified lherzolite in the system CaO–MgO–Al₂O₃–SiO₂–Na₂O from 7 to 35 kbar, *J. Petrol.* 35 (1994) 329–359.
- [64] M. Loubet, N. Shimizu, C.J. Allegre, Rare earth elements in alpine peridotites, *Contrib. Mineral. Petrol.* 53 (1975) 1–12.
- [65] P.B. Kelemen, N. Shimizu, T. Dunn, Relative depletion of niobium in some arc magmas and the continental crust: partitioning of K, Nb, La and Ce during melt/rock reaction in the upper mantle, *Earth Planet. Sci. Lett.* 120 (1993) 111–134.
- [66] N. Shimizu, I. Kushiro, The partitioning of rare earth elements between garnet and liquid at high pressures: preliminary experiments, *Geophys. Res. Lett.* 2 (1975) 414–416.
- [67] G. McKay, J. Wagstaff, S.-R. Yang, Clinopyroxene REE distribution coefficients for shergottites: the REE content of the Shergotty melt, *Geochim. Cosmochim. Acta* 50 (1986) 927–937.
- [68] J.G. Fitton, A.D. Saunders, L.M. Larsen, B.S. Hardarson and M.J. Norry, Volcanic rocks from the southeast Greenland Margin at 63°N: Composition, petrogenesis and mantle sources, in: Saunders, A.D., Larsen, H.C., Clift, P.D., Wise, S. (Eds.), *Proc. ODP Sci. Res. 152. Ocean Drilling Program*, College Station, TX, 1998, in press.
- [69] T.L. Grove, W.B. Bryan, Fractionation of pyroxene-phyric MORB at low pressure: an experimental study, *Contrib. Mineral. Petrol.* 84 (1983) 293–309.
- [70] S.-s. Sun, W.F. McDonough, Chemical and isotopic systematics of oceanic basalts: implications for mantle composition and processes, in: Saunders, A.D., Norry, M.J. (Eds.), *Magmatism in the Ocean Basins*, *Geol. Soc. Spec. Publ.* 42 (1989) 313–345.